J Multidisciplinary Scientific Journal

MDPI

Article

Self-Cooling Textiles—Substrate Independent Energy-Free Method Using Radiative Cooling Technology

Lea Zimmermann [1], Thomas Stegmaier [1,*], Cigdem Kaya [1] and Götz T. Gresser [1,2]

[1] German Institutes of Textile and Fiber Research (DITF), 73770 Denkendorf, Germany; lea.dorazimmermann@gmail.com (L.Z.); cigdem.kaya@ditf.de (C.K.); goetz.gresser@ditf.de (G.T.G.)
[2] Institute for Textile and Fiber Technologies (ITFT), University of Stuttgart, 70569 Stuttgart, Germany
* Correspondence: thomas.stegmaier@ditf.de

Abstract: Due to climate change, population increase, and the urban heat island effect (UHI), the demand for cooling energy, especially in urban areas, has increased and will further increase in the future. Technologies such as radiative cooling offer a sustainable and energy-free solution by using the wavelength ranges of the atmosphere that are transparent to electromagnetic radiation, the so-called atmospheric window (8–13 µm), to emit thermal radiation into the colder (3 K) outer space. Previous publications in the field of textile building cooling have focused on specific fiber structures and textile substrate materials as well as complex multi-layer constructions, which restrict the use for highly scaled outdoor applications. This paper describes the development of a novel substrate-independent coating with spectrally selective radiative properties. By adapting the coating parameters and combining low-emitting and solar-reflective particles, along with a matrix material emitting strongly in the mid-infrared range (MIR), substrate-independent cooling below ambient temperature is achieved. Moreover, the coating is designed to be easily applicable, with a low thickness, to ensure high flexibility and scalability, making it suitable for various applications such as membrane architecture, textile roofs, or tent construction. The results show a median daytime temperature reduction (7 a.m.–7 p.m.) of 2 °C below ambient temperature on a hot summer day.

Keywords: radiative cooling; substrate independent cooling; textile application; textile technology

Citation: Zimmermann, L.; Stegmaier, T.; Kaya, C.; Gresser, G.T. Self-Cooling Textiles—Substrate Independent Energy-Free Method Using Radiative Cooling Technology. *J* **2024**, *7*, 334–350. https://doi.org/10.3390/j7030019

Academic Editor: Antonio Gil Bravo

Received: 3 July 2024
Revised: 21 August 2024
Accepted: 22 August 2024
Published: 27 August 2024

1. Introduction

The heating of cities and settlements due to climate change and the associated overheating of the human body requires new materials and technologies to keep temperatures bearable.

Due to climate change, population increase, and the urban heat island effect (UHI), the cooling energy demand in cities increased by 23% from 1970 to 2010 [1].

Previous conventional cooling systems for buildings like air conditioners are based on thermodynamic cycles that account for a large share of electricity demand while dissipating waste heat and carbon dioxide (CO_2) into the environment [2].

Based on radiative cooling technology, materials can cool below ambient temperatures in a sustainable and energy-free way.

Radiative cooling is a common process in which a surface loses heat through thermal radiation. The largest entity utilizing radiative cooling to regulate its energy balance is the Earth itself, which is evident through phenomena like frost and dew formation on clear mornings. Figure 1a shows the radiant heat flow on the terrestrial surface. The Earth's surface temperature is approximately 300 K, while the cosmic microwave background of the universe exhibits a thermal blackbody spectrum at around 2.7 K. This temperature difference can be harnessed by emitting thermal infrared radiation through the atmospheric window into space. The transparency of the atmosphere is influenced and limited by gases such as carbon dioxide (CO_2), water vapor (H_2O), and ozone (O_3), which can reflect or absorb thermal radiation. However, within the atmospheric window, these gases have

negligible impact, permitting heat to be effectively radiated into space. Achieving daytime cooling requires materials with specific properties: high reflectivity in the solar spectrum (0.3–2.5 µm) and high emissivity in the atmospheric window (8–13 µm) (see Figure 1b). Effective daytime cooling is realized when the emitted thermal radiation exceeds the absorbed solar and atmospheric radiation [3].

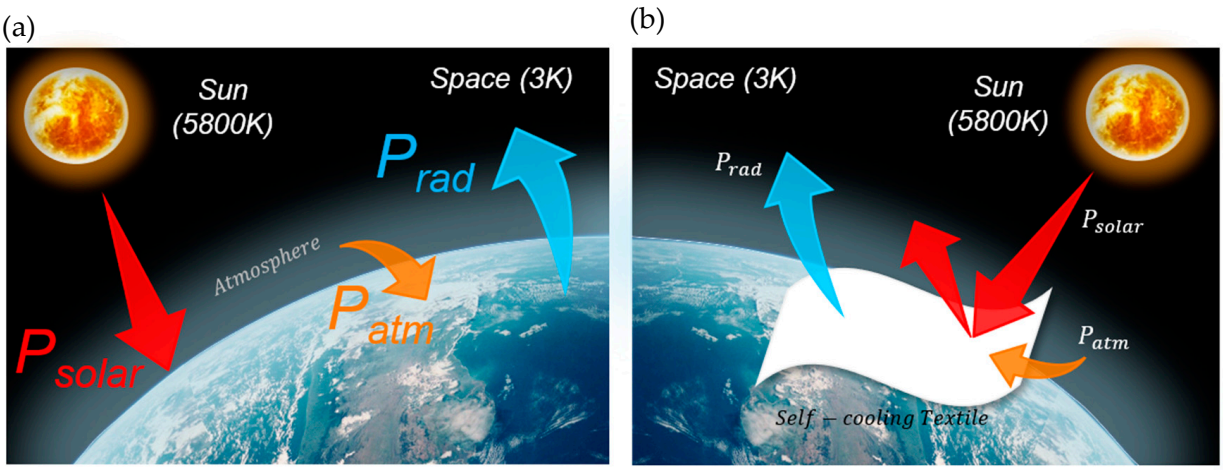

Figure 1. Schematic overview of radiative heat flows. (**a**) Radiant heat flows on the terrestrial surface; (**b**) Functional principle of a self-cooling material based on radiative cooling. (P_{solar}: solar radiation; P_{atm}: atmospheric downward-radiation; P_{rad}: thermal radiation between 8–13 µm).

Previous research on textile systems has primarily focused on personal thermal management through clothing. Direct cooling of the human body necessitates different material properties than those required for cooling a room or surface via technical textiles. Humans dissipate heat through evaporation, convection, and radiative cooling, with radiative cooling accounting for approximately 60% of heat transfer [4].

Innovations in personal cooling have explored thermally transparent materials, allowing the body to emit heat directly. Human skin is a proficient emitter in the mid-infrared (MIR), facilitating significant heat loss through radiative cooling [5]

Infrared-transparent clothing enhances this effect by enabling body heat to escape into the surrounding air. Reflective materials, such as zinc oxide particles [6], are used to reflect solar radiation and prevent additional heating of the body. Current materials, including nanoporous polyethylene (PE) [6–8] and natural alternatives like chitosan [9], have demonstrated temperature reductions of up to 5 °C compared to untreated textiles.

In the field of building cooling with textiles, research has focused on specific fiber structures [10–13], textile substrates [14–16], and complex multi-layer systems [13,17], achieving cooling of up to 5 °C below ambient temperatures. Textiles, depending on their material and area per weight, achieve relatively high broadband emission in the mid-infrared range, which can be used to emit heat through the atmospheric window. By designing textiles with scattering elements through random fiber deposition, porous structures, or reflective particles, effective cooling materials can be developed. However, scalability and industrial application are restricted due to material-specific dependencies, resulting in monofunctional limitations.

For flexible application scenarios and broad economic feasibility, the aim should be a substrate-independent application with a simple application process and sufficient cooling performance.

Substrate-independent material systems achieve consistent cooling across different substrates, with cooling properties derived from the coating components rather than the substrate material itself. However, few examples exist where textiles do not contribute to cooling performance explicitly to date.

Zhong et al. (2021) [14] described the modification of cotton fabric with aluminium phosphate particles bound to the fibers by O-Carboxymethylchitosan (CMC) and an additional hydrophobic PDMS layer, achieving a 5.4 °C temperature difference between uncoated and coated cotton. The cellulose does not contribute to the cooling performance. Ji et al. (2021) [18] investigated the influence of PDMS and PMMA in a two-layer coating on cotton fabric. The measurement shows a temperature reduction of 7.8 °C using a high layer thickness of 1.5–3.5 mm. The cotton serves only to protect the PMMA layer.

The Patent by Ningbo Radi-Cool describes a substrate-independent functional textile material with layer thicknesses of <250 µm and reflection and emission values $\geq$ 80%. This is achieved by combining varied solar reflective particle types and sizes. Nylon, polyester, and cotton are listed as possible textile substrates [19].

However, the described research often relies on complex and non-scalable application processes, suffers from reduced flexibility and practicality due to high coating thicknesses, or does not verify the cooling performance of different textile substrate materials.

In non-textile applications like paint and films, substrate independence has been more thoroughly investigated. Mandal et al. (2021) [20] described the influence of particle concentration and coating thickness on achieving high solar reflectance, with a minimum layer thickness of 300 µm required for PTFE-based coatings to achieve substrate independence. Various substrates like wood, metal, and plastic are tested. Li et al. (2021) [21] investigated a single-layer paint with $BaSO_4$ particles, achieving substrate independence at a thickness of 400 µm; below this thickness, the substrate influences infrared measurements.

Thick layers (400–1000 µm) [20,21] increase material consumption, reduce flexibility, and increase weight, which is crucial in textile applications.

Alternative approaches for thin layer applications include metalized films (e.g., silver or aluminium) [22–24]. To use metallizing films or layers in radiative cooling, a combination with a highly emissive material is required. Metal films reduce the transmissivity radically and, at the same time, increase solar reflectivity. However, these approaches face challenges regarding textile applications, such as manufacturing complexity, adhesion issues, and reduced longevity due to oxidation and abrasion [25,26].

This study aims to develop a novel substrate-independent coating with spectrally selective radiation properties based on thermo-optically active particles, generating a self-cooling effect on textile surfaces. The work builds upon the state of research on metalizing films and layers. To minimize time-consuming and cost-intensive process steps while ensuring high adhesion and flexibility of the coating, as well as to achieve simple coating application on various textile substrates, this work pursues the approach of directly integrating metalizing particles into the coating.

So far, the direct integration of low-e particles, such as aluminium, has been used to minimize the overall emission performance [27,28]. In the combination of Low-e and High-e materials, either no radiative cooling function is achieved, or the layers are used functionally separately [7,29].

The use of aluminium (Al) as a low-emissivity material directly implemented in a high-emissive matrix material is investigated to understand how low-e materials can help achieve substrate-independent cooling. The coating is applied to various textile substrates with different fibre materials and basis weights using a simple doctor blade coating technique.

2. Materials and Methods

2.1. Textile Substrate Materials

As textile substrate materials, we used three different standard fabrics, which are among the materials typically used in membrane and tent construction, in addition to ETFE [30].

A standard polyester fabric (UTT, Krumbach, Germany) with a weight per area of 65 g/m^2 (PES 65) was utilized as well as a standard polyamide fabric (UTT, Krumbach, Germany) with a weight per area of 150 g/m^2 (PA6.6 150) and a glass fabric (UTT, Krum-

bach, Germany) with a weight per area of 163 g/m^2 (Glass 163). Details of the materials used can be extracted from the Supplementary Materials Table S1.

For the basis weight, a comparatively very light fabric and a significantly heavier fabric were selected. This combination represents the wide range of strength classes in membrane and tent construction and results in high spectral differences. Details of the spectral curve can be extracted from the Supplementary Materials Figure S1. The percentage deviation of the spectral profile in the solar range between Glass 163 g/m^2 and PES 65 g/m^2 averages 47% over the wavelength range of 0.3–2.5 µm. In the mid-infrared range (2.5–20 µm), the average percentage deviation from PA6.6 to PES is 32.2%, providing three distinct different substrate textile materials based on their spectral profiles.

2.2. Coating Formulation

For the coating formulation of the cooling textile material, silicone (LR6250F, Wacker Chemie AG, Munich, Germany) is used as the matrix material. Silicone is a material that has already been used for radiative cooling applications in the textile area [10,14,31]. Due to the number of functional groups like Si-O-Si, the material exhibits specific vibration frequencies that result in emissivity peaks, especially within the atmospheric window (8–13 µm) [32]. It is mixed with the crosslinking agent (525, Wacker Chemie AG, Germany) in a ratio of 100:3.

The coating consists of two functional layers. The first layer is based on aluminium as an underlying material. Here, aluminium particles (ECKART GmbH, Hartenstein, Germany) are directly integrated into the silicone matrix. Various materials for particles have been defined and used as low-emitting (low-e), whereby the focus is on silver and aluminium due to their very good radiation-optical properties. Considering the requirement of economic feasibility and the associated more cost-effective production, the benefits of low-emitting particles are examined and highlighted in this work using the example of aluminium.

For the second layer, white pigments like TiO_2 (The Chemours Company, Wilmington, DE, U.S.A.) are added. TiO_2 particles reach, based on their refractive index, particle size, and particle distribution, a high solar reflectivity, especially in the visible range [33–35]. TiO_2 also serves as a reference material to investigate the influence of low-e materials in the combined coating system.

The coatings are stirred for 3 min at 800 rpm to achieve a uniformly distributed paste. Figure 2 provides a schematic overview of the past preparation process.

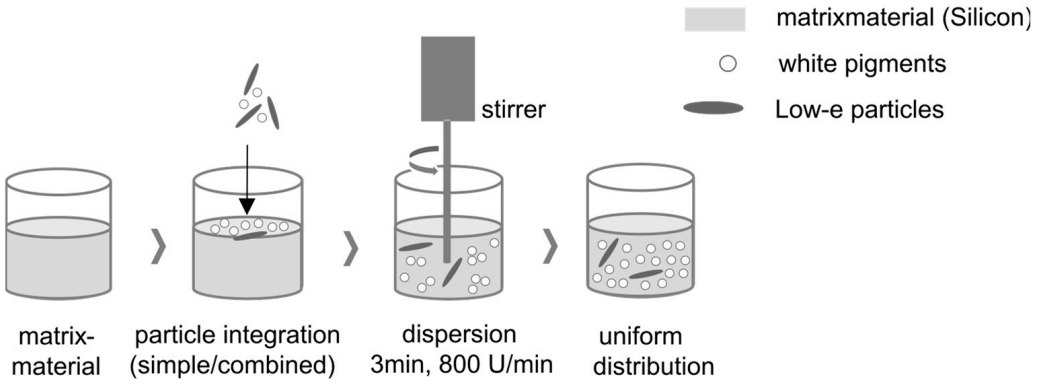

Figure 2. Schematic representation of the paste preparation steps.

2.3. Coating Application

The prepared coating pastes are applied to various textile substrates using the Mathis Labcoater (Werner Mathis AG, type no. LTE-S M 68404, Oberhasli, Switzerland). Initially, the first paste is applied onto the textile substrate using the doctor blade technique, then dried for 3 min at 100 °C and crosslinked for 3 min at 150 °C using the Mathis Labdryer

(Werner Mathis AG, type no. LTE-S M 68404, Switzerland). The doctor blade method is a well-established process in the textile industry for applying coating pastes to textile substrates, ensuring subsequent scalability and economic producibility. Following this, the second functional layer is added directly onto the first cured layer using the same process.

Figure 3 provides a schematic overview of the coating application process.

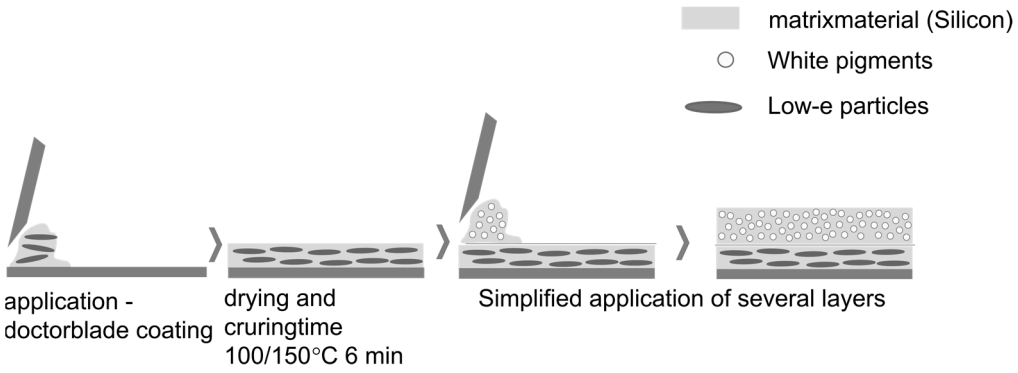

Figure 3. Schematic representation of the coating application steps. Coating application on textile substrate materials using the doctor blade method, either single or multilayered.

The thickness of the coated layers is determined by the application thickness. This is set on the Mathis Labcoater using dial gauges with an adjustment accuracy of 0.01 mm. To measure the coating thickness more precisely, the cross-section of the sample is imaged and analyzed using a scanning electron microscope (SEM) (TM1000, Hitachi Ltd., Tokyo, Japan). The layer thickness is determined from the distance between material boundary lines in the recorded material profile, allowing for precise measurement of each layer's thickness even in multi-layer applications.

2.4. Spectral Measurements

The solar reflectivity and transmissivity in the range of 0.3–2.5 µm are obtained using an ultraviolet–visible–near-infrared (UV–Vis–NIR) spectrometer (LAMDA 1050+, Perkin Elmer Ltd., Shelton, CT, USA), while the infrared emissivity in the range of 2.5–20 µm is measured using a Fourier transform infrared (FTIR) spectrometer (Vertex 80, Bruker Corporation, Billerica, MA, USA.). For reflectance standardization, an integrating sphere coated with highly diffuse reflective materials is employed. In the Lambda 1050+ spectrometer, a 150 mm InGaAs (Indium-Gallium-Arsenide) detector and an integrating sphere with a Spectralon® inner coating are used. Before each new series of measurements, a baseline reading with T% = 100 is performed using the calibration standard Spectralon® (Labsphere, North Suttin, NH, USA).

In the Vertex 80, a gold-coated integrating sphere with a DLaTgs (Deuterated L-Alanine doped Triglycine Sulfate) detector is used. Before each new series of measurements, a background measurement is taken using the gold standard without the sample.

The measurements are conducted at room temperature using a sample size of 5 cm × 5 cm. The measurement procedure follows ASTM E 903:2020 [36] (Standard Test Method for Solar Absorptance, Reflectance, and Transmittance of Materials Using Integrating Spheres).

2.5. Outdoor Test Module

To measure the temperature differences as well as the cooling power under real weather conditions, a test was built on the roof of the German Institutes for Textile and Fiber Research (DITF) (48°42′02.6″ N, 9°20′36.8″ E).

Two test setups have been designed, each differing slightly in their approach. The first setup (see Figure 4a) focuses on comparing the thermal properties of various materials. This setup has been designed to accommodate a larger number of measurement points, allowing multiple materials to be examined simultaneously under identical conditions.

A total of six test modules are set up. The sample area, which is oriented towards the sky, is 25 ± 0.5 cm^2. A detailed description and schematic overview can be obtained from Supplementary Materials Figure S2.

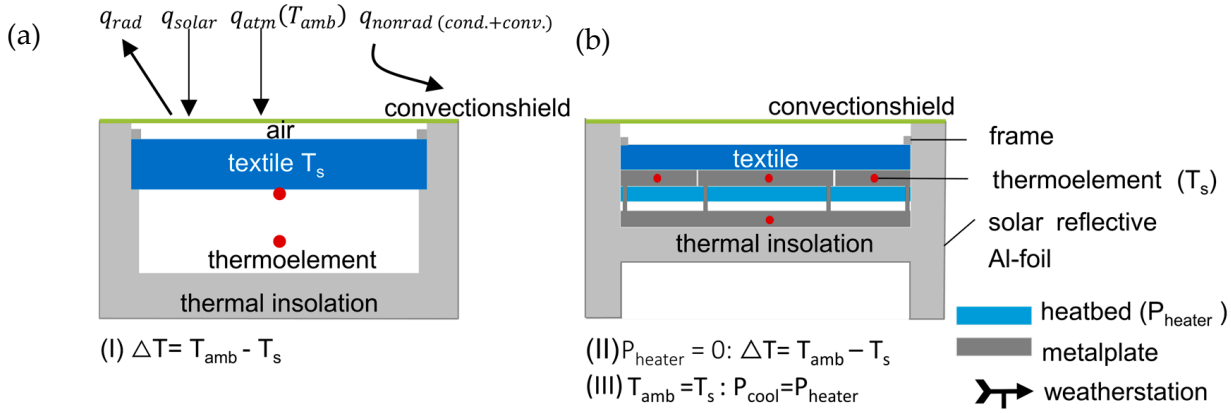

Figure 4. Schematic representation of the test modules. (**a**) Temperature measurement: $\triangle T = T_{amb} - T_s$; (**b**) Cooling power measurement with a feedback-controlled heating plate system: $P_{heater} = 0$.

Two thermocouple sensors NiCr-Ni (Ahlborn Mess- und Regelungstechnik GmbH, Holzkirchen, Germany) of type K are used as temperature sensors in each test setup. One temperature sensor is located in the center directly below the sample. A second sensor is fixed exactly in the center of the box. The temperature sensors are read out using a data logger 710 (Ahlborn Mess- und Regelungstechnik GmbH, Germany) and the AMR WinControl software V9.0.3.0 (Ahlborn Mess- und Regelungstechnik GmbH, Germany). The cooling capacity can be determined using method (I) $\Delta T = T_{amb} - T_s$ measuring the temperature of the cooling sample T_s and the air temperature T_{amb} to represent the cooling performance in relation to the ambient temperature in degrees Celsius.

In contrast, the second setup (see Figure 4b) is geared towards quantifying the actual cooling capacity in watts per square meter. For this purpose, two identical setups incorporate integrated heating plate systems. This configuration enables the measurement of a reference material alongside the sample material for comparative analysis. By implementing a feedback-controlled heating plate system, the cooler temperature (T_s) is kept equal to the ambient temperature (T_{amb}). The cooling capacity can be determined using method (II), where the heating power P_{heater} is set to zero so that the maximum temperature reduction of the sample can be measured ($\Delta T = T_{amb} - T_s$). To measure the cooling performance in W/m^2, Method (III) uses the feedback system to maintain the temperature of the cooling material at the constant level of the ambient temperature ($T_{amb} = T_s$), so that the net cooling power (P_{cool}) can be determined by the initiated heating power ($P_{cool} = P_{heater}$). The temperature difference between the environment and the textile sample is kept to less than 0.2 °C throughout the entire measurement period. By implementing a "Guarded-Ring" system separating the metal plate into a core and a frame plate based on the standard test method for thermal conductivity (Guarded-Hot-Plate) [37], a one-dimensional heat transfer between the core and the sample is ensured, and side losses are limited [38]. The measuring area of the core and, thus, the surface of the material is 100 ± 0.5 cm^2. To measure the cooling capacity in watts per square meter, self-adhesive silicone heating mats (RS Components GmbH, Frankfurt am Main, Germany) are attached below the metal plates. The heating mats are connected to the power supply unit HMP4030 3-CH (Rohde & Schwarz, Munich, Germany). The thermocouples NiCr-Ni (Ahlborn Mess- und Regelungstechnik GmbH, Germany) of type K temperature sensors are placed in the metal plate so that the measuring tip sits exactly in the middle of the respective plate. Due to the low thickness of the aluminium plate, the exact temperature of the heating plate, and thus T_s can be determined. For the frame plate, two temperature sensors are used, and the average value

is calculated from this. The schematic representation of the test modules can be seen in the Supplementary Materials Figure S3.

To further reduce influences from convection or conduction, both test setups (Figure 4a,b) are insulated using expanded polystyrene (styrofoam). The Styrofoam is equipped with solar-reflective self-adhesive aluminium foil (Calorique, Düren, Germany) both on the inside and outside to reduce conduction. To protect the measurement from the influence of convection, a convection shield made of polyethylene (low-density polyethylene (LDPE)) with a thickness of 10 ± 5 µm is also applied. Two temperature sensors are used to measure the ambient temperature (see Supplementary Materials Figure S3). A thermocouple sensor NiCr-Ni (Ahlborn Mess- und Regelungstechnik GmbH, Germany) of type K is mounted at the height of the test modules. The measuring tip is covered with a reflective foil (aluminium) so that it is protected from direct sunlight, and at the same time, an unobstructed airflow is ensured. A digital sensor for measuring humidity, temperature, and air pressure (FHAD46C41AL05, Ahlborn Mess-und Regelungstechnik GmbH, Germany) is also mounted in a climate housing (Technoline, Wildau, Germany) at the height of the test modules. The climate housing, similar to a Stevenson screen, also serves to shade the temperature sensor and, at the same time, ensures a free flow of air through the slat openings. The ambient temperature is averaged from both sensors.

The meteorological data, such as humidity, wind strength, solar irradiance, or air pressure, are measured by a weather station located approximately three meters away from the test setups on the rooftop of the institute. The test setups are mounted approximately one meter above the roof surface so that the heat radiation from the ground does not have a significant impact on the measurement.

Details regarding used devices, uncertainties, and materials can be extracted from Tables 1 and 2.

Table 1. Used Devices and their uncertainty for the measurement setup.

Devices	Model	Uncertainty
Thermoelement NiCr-Ni	Typ K	±1.5 K
Digital sensor for humidity, temperature, air pressure	FHAD46C41AL05	±0.2 K
Data logger	ALMEMO® 710	-
Meteorological sensor for wind	FMD760	±0.3 m/s
Meteorological sensor for humidity	FMD760	±2%
Meteorological sensor for air pressure	FMD760	±0.5 hPa
Global radiation sensor for UVA, VIS, IR-radiation	FLA613T1B11	<10%
Pyranometer	CM 11	<10 W/m^2

Table 2. Used Materials and their thickness in the measurement setup.

Material	Thickness
Insulation (styrofoam)	10 ± 0.5 cm
Solar reflective aluminium foil (Calorique, Germany)	30 ± 5 µm
Metal plate (aluminium)	0.6 ± 0.05 cm
Silicone heating mats (RS Components GmbH, Germany)	1.4 mm
Windcover—Polyethylene (LDPE)	10 ± 5 µm

To ensure comparability between the different test modules, the variability was checked by using aluminium foil as a sample for both test setups. The temperature of the test modules was measured during the day over a period of 40 min. A slight average deviation of 0.3 °C was measured at an average direct solar radiation of <400 W/m^2. The deviation is within the range of the measurement accuracy of the temperature sensors so that the test modules can be regarded as identical. The result can be seen in Supplementary Materials Figure S4.

2.6. Longevity Measurement Outdoors

The coated samples were placed outdoors on the rooftop of the institute for up to five months, starting from July 2023 until early December 2023. The samples were measured before the outdoor exposure using the spectral measurement devices described in Section 2.5. After the outdoor exposure period, the samples were measured again to evaluate the impact of weathering on their performance and longevity.

3. Results

3.1. Influence of Low-e Particles on Spectral Curve

3.1.1. Influence on Solar Transmissivity

The following concentrations for aluminium particles were investigated: 5, 10, 20, and 30 wt.%. To compare the impact of aluminium particles directly integrated into silicone as a high-emissive matrix material, we investigated the spectral impact of standard white pigments like TiO_2 in the same coating structure. TiO_2 was investigated with concentrations of 20, 30, 40, 50, and 60 wt.%. According to the literature, an optimum particle concentration distribution is considered to be at 30–40 wt.% [33]

The particles are evenly distributed in the matrix material silicone and applied with a coating thickness of 100 ± 15 µm onto the textile substrate material. The spectral curve measured in the solar range shows the impact of the particle concentration on the solar transmissivity value (see Figure 5).

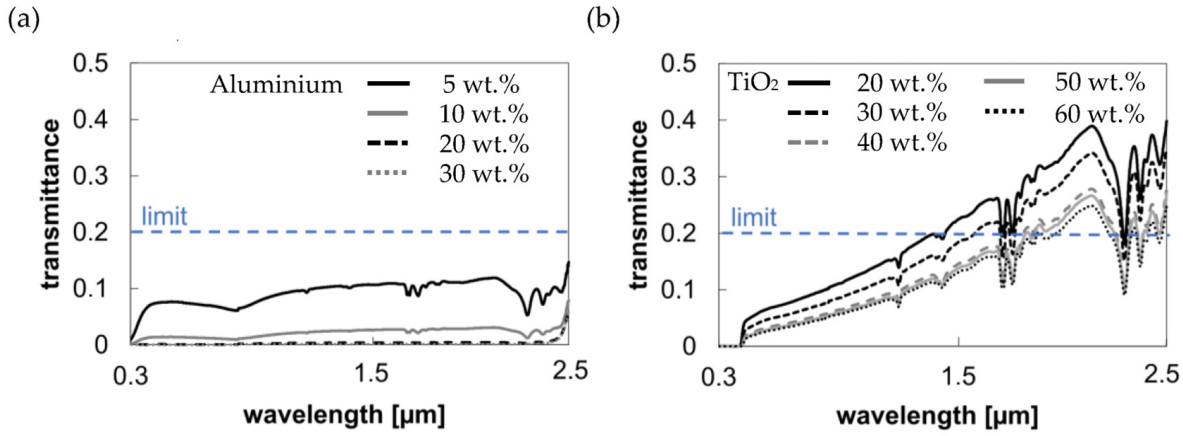

Figure 5. Concentration-dependent solar transmission using the example of Glass 163 g/m^2. The limit value is defined according to Nagshine and Saboonchi [39]. (**a**) Solar transmittance as a function of the aluminium particle concentration (layer thickness: ∅ 94.35 ± 7.13 µm); (**b**) Solar transmittance as a function of the titanium dioxide concentration (layer thickness: ∅ 95.4 ± 7.73 µm).

An aluminium particle concentration of 20 wt.% reduces the solar transparency to less than 1%. At the same time, TiO_2 as a reference material does not reduce the transmission in the solar range below the defined threshold of 0.2, even with high particle concentrations of 60 wt.%.

The higher the transmissivity value, the greater the impact of the underlying materials will be. The threshold value of 0.2 is defined by B. Nagshine and A. Saboonchi [39], who investigated the cooling power with black background materials. Above 0.2, a positive cooling power combined with a black background material is not achievable. Thus, by reducing the overall transparency, the substrate material has less influence on the overall cooling performance, resulting in substrate independence.

3.1.2. Influence in the Mid-Infrared Range

Aluminium particles can also have a significant concentration-dependent influence on the spectral curve in the mid-infrared range.

Figure 6 shows the spectral curve of the emission between 2.5–15 µm, which is determined from the measured transmission and reflection spectrum by E = 1 − R − T.

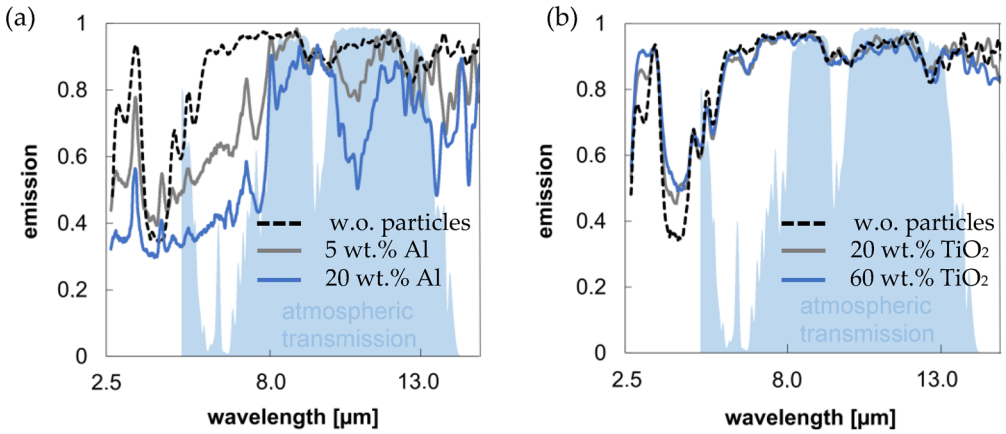

Figure 6. Influence on the spectral response in the MIR as a function of particle type and concentration using the example of PES 65 g/m^2. (**a**) Emission in the MIR as a function of the aluminium particle concentration; (**b**) Emission in the MIR as a function of the titanium dioxide particle concentration.

The respective lowest and highest particle concentrations are shown here. Additionally, the spectrum of the textile coated only with the matrix material, silicone, without (w.o.) the addition of particles, is presented as a reference sample. The addition of aluminium particles in the high-emitting silicone system influences the emission curve in the mid-infrared range (especially between 2.5–13 µm), depending on the concentration. Despite the material-specific low emission value of low-e materials, a total emission power in the atmospheric window (8–13 µm) of >75% (see Figure 6a) is reached. Thus, the direct integration of metal particles in a highly emissive material like silicone can result in a reasonably high emission power. Additionally, aluminium particles can reduce the absorption outside the atmospheric window between 2.5–8 µm depending on the concentration, leading to lower absorption of atmospheric radiation.

In contrast, TiO_2 particles have no significant influence in the mid-infrared range. The curve remains similar to that of the textile coated with silicone without particles included (see Figure 6b).

3.2. Substrate Independent Spectral Measurement by Two-Layer System

Based on our material screening and previous test results, the overall solar reflectivity by integrating aluminium particles does not exceed 70%. This is due to a higher scattering factor compared to, for example, a polished metal layer. Specifically, in the visible range, there is a slight decrease in solar reflectivity. To achieve high solar reflectivity, a second layer with TiO_2 particles is integrated. Using the same application method (described in Section 2.3), the production process remains simple and scalable to large textile surfaces. To ensure sufficient flexibility, the total coating thickness is defined to be less than 300 µm.

3.2.1. Influence Low-e Particles in a Two-Layer System

By comparing the same coating structure with and without the integration of aluminium particles, the influence in a two-layer system can be spectrally analyzed. Figure 7 shows the advantage of the additional integration of aluminium particles, especially in the near-infrared range and in the reduction of solar transmission. TiO_2 exhibits high reflectivity in the visible range but absorbs increasingly in the near-infrared range, depending on the particle concentration. In this wavelength range, TiO_2 is also significantly more transparent, allowing solar radiation to pass through the coating and textile, potentially warming the spaces beneath. Applying a first layer with low-emissivity (Low-e) particles minimizes this disadvantage.

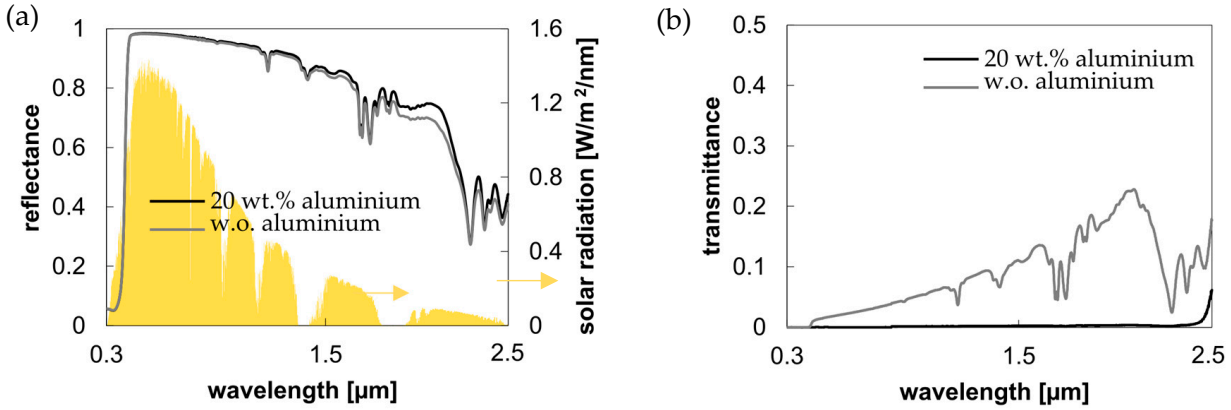

Figure 7. Influence of the Al particles on the spectral response compared to the reference coating. Coating thickness first layer: 60 ± 10 µm, particle concentration first layer: 20 Wt.% aluminium; coating thickness second layer: 200 ± 15 µm, particle concentration second layer: 40 Wt.% TiO_2 on PES 65 g/m^2. Reference coating: first layer: 60 ± 10 µm w.o. particles, second layer: 200 ± 15 µm with 40 Wt.% TiO_2 on PES 65. (**a**) Solar reflectance; (**b**) Solar transmittance.

The solar reflection in the near-infrared range (between 1.5–2.5 µm) is increased by an average of 3.3% due to the aluminium content. Meanwhile, the solar reflectance in the visible range, based on the TiO_2 concentration and the two-layer structure, averages 96.6%, which is well above 90%.

3.2.2. Substrate Independent Spectral Measurement

To investigate the substrate independence, the coating is applied to three different textile substrate materials. The scanning electron microscope image in Figure 8a–c shows the applied coating on each textile substrate material. The spectral curve indicates no significant difference based on the substrate textile material, suggesting that the textile itself does not significantly influence the coating's performance (see Figure 8d,e).

The emission between 8–13 µm is 94% for all three substrates and therefore well above 90%. The solar reflectivity reaches a maximum of up to 98%.

The incoming light is scattered and reflected by the TiO_2 particles in the first layer. Light that reaches the second radiation-functional layer is reflected by the aluminium particles, preventing any light from being transmitted through the first two layers to the textile substrate. This eliminates the influence of the substrate. A more detailed schematic overview of the microstructure of the coating is provided in Figure S5 in the Supplementary Materials.

In a coating application without aluminium content, substrate differences can be reduced due to a higher layer application and, thus, higher particle volume concentration (see Table 3). However, differences in the spectral curve are still noticeable (see Supplementary Materials Figure S6), which can result in variations in the overall cooling performance.

Table 3. Summary of the results of coating application with aluminium particles compared to reference systems. Average values of solar transmission and reflection as well as emission between 8–13 µm using the example of PES 65, PA6.6 150, and Glass 163.

R_{solar} (%)/T_{solar} (%)/$\varepsilon_{8–13\ \mu m}$ (%)	PES 65 g/m^2	Glass 163 g/m^2	PA6.6 150 g/m^2
Reference without coating	29.1/62.6/67.5	55.0/43.9/92.5	41.6/42.1/91.6
Reference without Al-particles	75.8/8.76/91.9	76.2/8.99/92.4	75.7/5.32/92.4
Coating with Al-particles	**77.4/0.24/94.1**	**77.3/0.27/94.5**	**76.9/0.22/94.0**

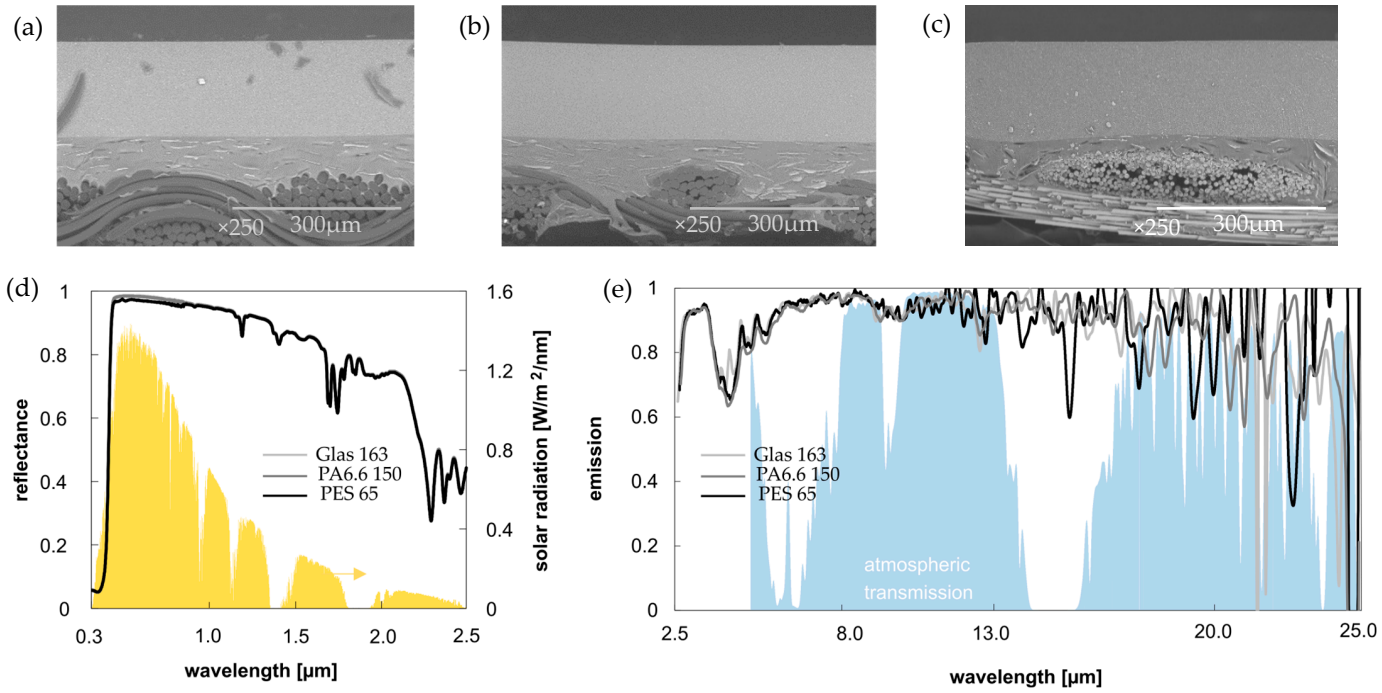

Figure 8. Optical and spectral investigation of substrate independence. (**a**) PA6.6 150 g/m^2, layer thickness: 1st layer: 65.84 ± 11.36 µm, 2nd layer: 194.39 ± 5.97 µm; (**b**) PES 65 g/m^2, layer thickness: 1st layer: 64.93 ± 10.14 µm, 2nd layer: 187.80 ± 3.46 µm; (**c**) Glass 163 g/m^2, layer thickness: 1st layer: 60.52 ± 18.14 µm, 2nd layer: 187.80 ± 3.46 µm (SEM TM1000 × 250, Hitachi); (**d**) Solar reflection; (**e**) Emission in MIR with the atmospheric window between 8–13 µm.

The following Table 3 summarizes the results of the measured solar reflection, transmission, and mid-infrared (MIR) emission for all three substrates.

3.3. Measurements under Real Weather Conditions

The temperature difference is measured for the coated and uncoated system on three different substrate materials PES 65, Glass 163, and PA6.6 150 for >24 h (see Figure 9).

To ensure that all test modules have a comparable initial temperature, the samples were covered with aluminium foil before each new measurement series. The removal of the aluminium foil, marking the start time of the measurement, is indicated with a dashed line in the graph.

Figure 9 shows that the temperature of the coated samples remains nearly identical throughout the test period. An average daily deviation of 0.25 °C was measured, which falls within the specified measurement accuracy. The coated samples maintain average daily temperatures of 19.8, 20.0, and 20.0 °C for PES 65, Glass 163, and PA6.6 150, respectively.

The ambient temperature averages 22.7 °C over the course of the day, resulting in an average temperature reduction of approximately 2.7 °C compared to ambient conditions. Even with solar irradiance exceeding 1000 W/m^2 at midday, the temperature curve remains at or below the ambient temperature and shows no warming above T_{amb}.

An average temperature reduction of 13.5, 10.6, and 11.1 °C was achieved for PES 65, Glass 163, and PA6.6 150, respectively, for the coated samples during the day (7 a.m. to 7 p.m.) compared to the uncoated fabrics.

Thus, cooling below the ambient temperature during the day is achieved with the coating system regardless of the substrate material.

Besides the temperature reduction, the cooling power was measured using the feedback heating system. By using two identical test setups, the maximum temperature reduction and cooling power can be measured under the same ambient conditions. Figure 10 shows the maximum temperature reduction at midday compared to the ambient temper-

ature. At the same time, a positive cooling power is measured, resulting in an average cooling power of 43 ± 10 W/m^2.

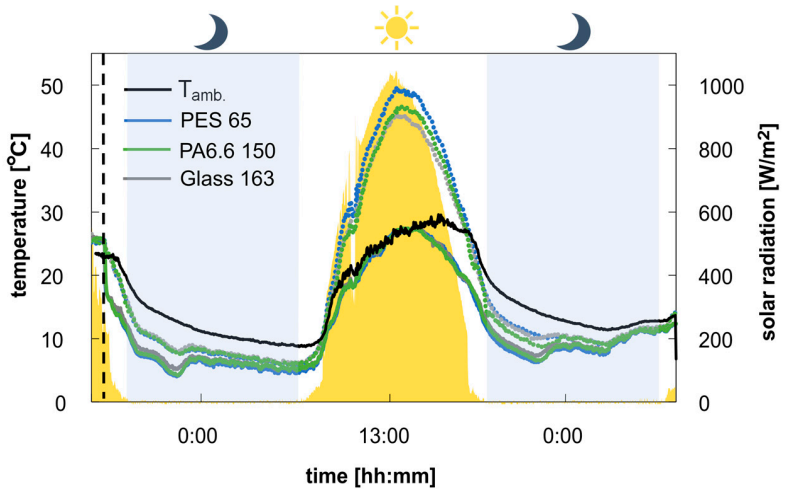

Figure 9. Temperature measurement on different substrates under real weather conditions over a period of >24 h. Solid line = coated substrate; dotted line = uncoated substrate (reference sample). Measured with the test module for pure temperature measurement from 19 September 2023–21 September 2023 on the roof of the DITF. Maximum solar irradiation during the day (20 September 2023): 1046.1 W/m^2, average wind speed during the day (7:00–19:00): 0.7 m/s, average relative humidity during the day (7:00–19:00): 59.3%.

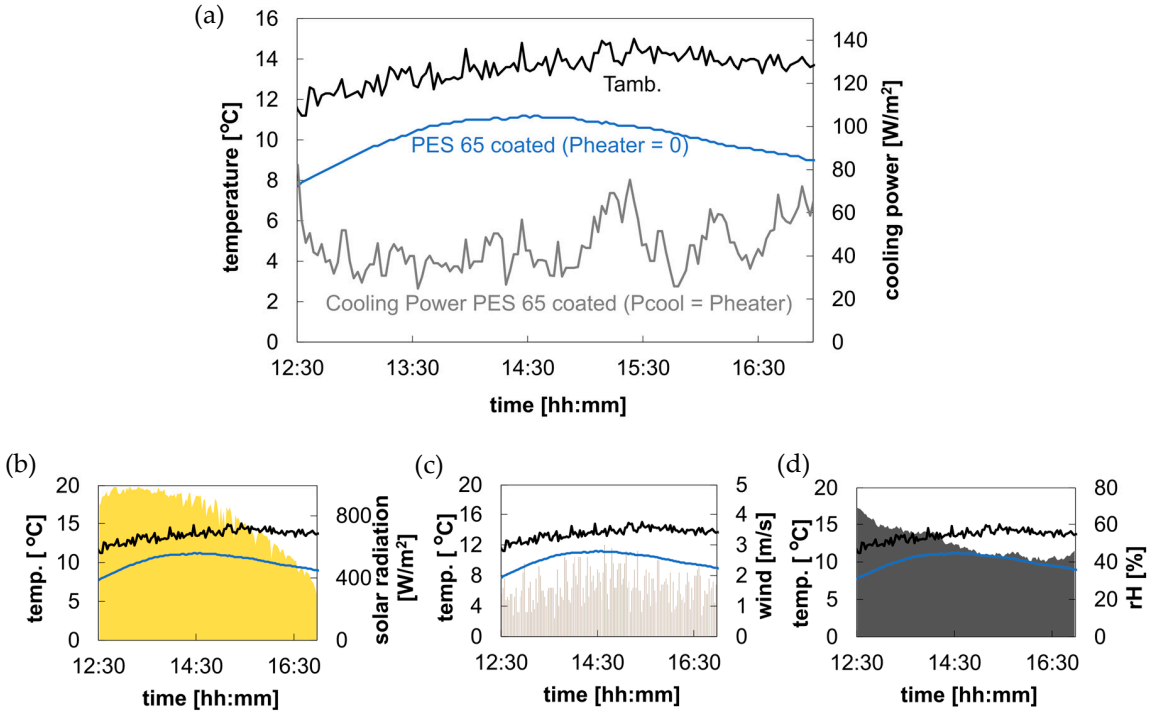

Figure 10. Maximum temperature reduction and cooling power of the coated sample during the day. Sample: PES 65 g/m^2 coated (total coating thickness: 250 ± 20 µm). Representation of the heat input (P_{heater}) by the average period 10 at 150 data points. Measured with the test module with integrated heating plate system on 16 October 2023 on the roof of the DITF. (**a**) Temperature profile and cooling capacity of the samples; (**b**) Temperature of the sample and T_{amb}; against solar radiation (max. 995.5 W/m^2); (**c**) Temperature of the sample and T_{amb}; against the average wind speed (Ø 1.7 m/s); (**d**) Temperature of the sample and T_{amb} against the relative humidity (Ø 50.0%).

3.4. Longevity Measurement

To investigate the long-term functionality of the samples, they were exposed to outdoor weathering for a period of 5 months. Figure 11 illustrates the sample surface throughout the measurement period. During this time, the samples experienced extreme temperatures and weather conditions. In July 2023, temperatures reached up to 43 °C. November 2023 was the wettest month since 2017, and in December 2023, temperatures occasionally dropped below zero (−3 °C), accompanied by snowfall.

Figure 11. Longevity measurement. Sample: PES g/m^2 coated (total coating thickness: 250 ± 20 µm).

The coated surface is water-repellent, so raindrops can wash away some of the attached dirt. August was a relatively dry and dusty month, during which most of the dirt particles attached to the surface. After wiping the right side clean again, it remained relatively clean over the next couple of months, demonstrating a certain self-cleaning effect due to the high hydrophobicity of the silicone coating.

After cleaning the sample that was exposed to outdoor weather conditions, the solar reflection returned to the level and condition of the sample prior to weathering (see Figure 12). This demonstrates that the coating can provide consistent cooling in the long term. The silicone coating was chosen not only for its high emissivity but also to ensure weather stability. The matrix material is UV stable and hydrophobic, protecting the integrated particles inside.

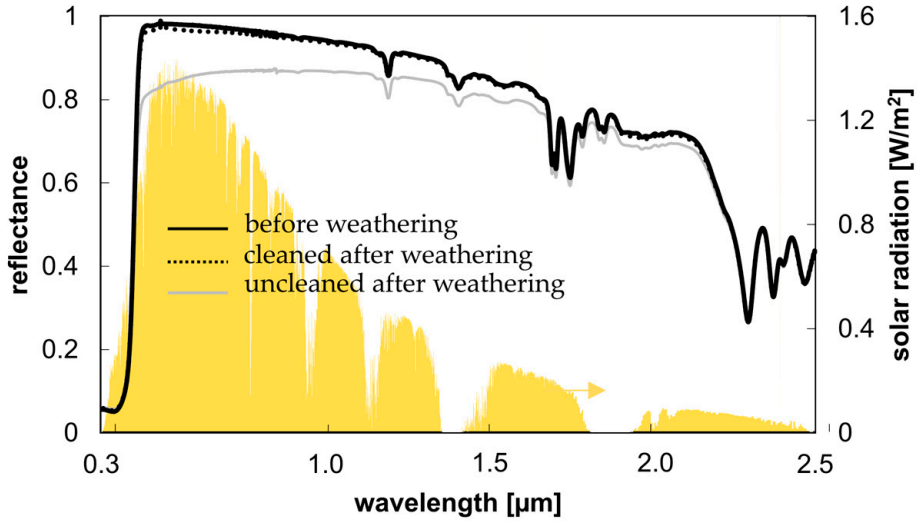

Figure 12. Spectral measurement and comparison of solar reflectance before weathering, cleaned after weathering and uncleaned after weathering. Sample: PES g/m^2 coated (total coating thickness: 250 ± 20 µm).

Dust particles on the sample surface can significantly reduce solar reflection in the visible range, but the reflection value of 70% is still significantly higher than that of the uncoated comparison textile. However, cleaning the surface is recommended to maintain consistently high cooling performance over the long term.

4. Discussion

This research provides an innovative approach to achieving large-scale, low-cost, and multifunctional applications for textile systems. The results demonstrate that the coating can be applied to different textile substrates, generating an identical cooling effect and confirming its versatility. This adaptability is crucial for various applications, ensuring that the solution is effective across different materials and consistently achieves significant temperature reductions, even during hot summer days.

One of the major advantages of textile systems is their mobility. For example, in shading systems for buildings, textiles can be deployed when cooling is needed and removed when it is not. This mobility contrasts sharply with fixed solutions like roof paints, which provide continuous cooling, even during winter when it may be less necessary, especially in temperate regions. This ability to deploy and retract cooling textiles as needed highlights the importance of finding functional and versatile textile solutions.

By incorporating low-emissivity particles directly into the coating formulation, the limitations associated with structure-based textiles and metal coatings, such as reduced variability or complex process steps and vulnerability to abrasion effects, are avoided. Metal particles can offer a decisive advantage in terms of substrate independence and increased NIR reflection, especially with low layer thicknesses (<300 µm). Additionally, adjusting the particle concentration allows the coating to be tailored to specific requirements, such as achieving higher or lower solar transmission in the visible range for varying degrees of blackout effects.

The coating shows an emission performance of >95%, particularly in the atmospheric window, which is comparable to or even higher than the values reported in the literature, as described in Section 1. The reflection value, reaching up to 98% with an average value of approximately 80%, aligns with the values measured by RadiCool [18].

A direct comparison of temperature measurements in the state of research is difficult due to different measurement methods and environmental influences on the overall radiative cooling mechanism. To assess the cooling performance, it is important to consider external influences and observe how the temperature compares to the surrounding ambient temperature. With an average temperature reduction of approximately 2.7 °C compared to ambient conditions, the coating achieves sufficient cooling during hot summer days.

While the low layer thickness may limit further increases in cooling performance, this coating application is lighter and enables simple three-dimensional shaping. The potential good flexibility of the coated sample can be seen in the Supplementary Materials, Figure S7. This feature is particularly advantageous for textile application scenarios such as membrane or tent construction, enhancing economic feasibility. The results also highlight the importance of considering the longevity and functionality of the coating under real weather conditions. Achieving high cooling values is essential, but it is equally important to use materials that are not degraded by solar radiation or other weather influences. Sustainability requires that materials possess a certain durability, allowing the coating to provide long-term cooling.

In the future, it is crucial to apply these coatings in real-world scenarios on a large scale. Understanding when the coatings contribute positively and when they do not will be a critical next step in transitioning from research to real-world applications. A recently published article by Wu et al. in *Science* [40] demonstrated a radiative cooling textile incorporating silver nanofibers, which enhances thermal reflectivity by rejecting incoming heat from nearby buildings. This suggests that an additional metal particle layer in our coating could also contribute to higher thermal reflectivity, particularly in urban environments, which needs to be investigated further. These steps are vital

for developing products that can be used effectively and have a positive impact on creating a sustainable and cooler future, particularly given the extreme heat events already occurring worldwide.

5. Conclusions

In conclusion, this study has demonstrated a promising approach to multifunctional, sustainable cooling solutions using textile systems. By addressing both the technical challenges and practical considerations for large-scale application, this research paves the way for innovative cooling textiles that can be adapted to various needs and environments. The next steps will involve further refining these coatings for durability and efficiency in diverse real-world conditions, ensuring that they provide a reliable and effective solution to combat heat and improve comfort sustainably.

Supplementary Materials: The following supporting information can be downloaded at https://www.mdpi.com/article/10.3390/j7030019/s1, Figure S1: Spectral curves of the uncoated substrate textile materials.; Figure S2: Setup of the test modules for comparing different materials and measuring temperature differences.; Figure S3: Assembly of the test modules for measuring cooling performance in Celsius and W/m^2 using a feedback-controlled heating plate system.; Figure S4: Comparison of the test modules. Temperature measurement over a period of 40 min with identical sample usage.; Figure S5. Optical representation of the microstructure and the structure of the coating; Figure S6: Spectral investigation and advantages of the aluminium (Al) particle integration compared to the reference system without aluminium particles.; Figure S7: Flexibility test; Table S1: Specifications of the textile fabrics used as the substrate material.

Author Contributions: Conceptualization, L.Z., C.K. and T.S.; Methodology, L.Z.; Data curation, L.Z.; Visualization, L.Z.; Supervision, C.K., T.S. and G.T.G.; Writing—original draft preparation, L.Z.; Writing—review and editing, C.K., T.S. and G.T.G. All authors have read and agreed to the published version of the manuscript.

Funding: This research was funded through a doctoral scholarship awarded to L. Zimmermann by the Ingeborg-Gross Foundation. The test setup was also funded by the Ingeborg-Gross Foundation.

Institutional Review Board Statement: Not applicable.

Informed Consent Statement: Not applicable.

Data Availability Statement: Datasets generated in this work are available upon request.

Conflicts of Interest: The authors declare no conflicts of interest. The funders had no role in the design of the study; in the collection, analyses, or interpretation of data; in the writing of the manuscript; or in the decision to publish the results.

References

1. United Nations (Ed.) *World Urbanization Prospects: The 2018 Revision*; United Nations: New York, NY, USA, 2019; ISBN 978-92-1-148319-2.
2. Raman, A.P.; Anoma, M.A.; Zhu, L.; Rephaeli, E.; Fan, S. Passive Radiative Cooling below Ambient Air Temperature under Direct Sunlight. *Nature* **2014**, *515*, 540–544. [CrossRef]
3. Zhao, D.; Aili, A.; Zhai, Y.; Xu, S.; Tan, G.; Yin, X.; Yang, R. Radiative Sky Cooling: Fundamental Principles, Materials, and Applications. *Appl. Phys. Rev.* **2019**, *6*, 021306. [CrossRef]
4. Peter, D.; Erwin Joseph, S. (Eds.) *Physiologie*; 3. Auflage; Urban und Fischer: München, Germany, 1999; ISBN 978-3-437-41316-2.
5. Cheng, Z.; Han, H.; Wang, F.; Yan, Y.; Shi, X.; Liang, H.; Zhang, X.; Shuai, Y. Efficient Radiative Cooling Coating with Biomimetic Human Skin Wrinkle Structure. *Nano Energy* **2021**, *89*, 106377. [CrossRef]
6. Cai, L.; Song, A.Y.; Li, W.; Hsu, P.-C.; Lin, D.; Catrysse, P.B.; Liu, Y.; Peng, Y.; Chen, J.; Wang, H.; et al. Spectrally Selective Nanocomposite Textile for Outdoor Personal Cooling. *Adv. Mater.* **2018**, *30*, e1802152. [CrossRef]
7. Hsu, P.-C.; Liu, C.; Song, A.Y.; Zhang, Z.; Peng, Y.; Xie, J.; Liu, K.; Wu, C.-L.; Catrysse, P.B.; Cai, L.; et al. A Dual-Mode Textile for Human Body Radiative Heating and Cooling. *Sci. Adv.* **2017**, *3*, e1700895. [CrossRef]
8. Iqbal, M.I.; Lin, K.; Sun, F.; Chen, S.; Pan, A.; Lee, H.H.; Kan, C.-W.; Lin, C.S.K.; Tso, C.Y. Radiative Cooling Nanofabric for Personal Thermal Management. *ACS Appl. Mater. Interfaces* **2022**, *14*, 23577–23587. [CrossRef]

9. Chen, C.; Jia, X.; Li, X.; Shi, M.; Hu, J.; Song, M.; Wu, S.; Dai, H.; Wang, X.; Geng, H. Scalable Wet-Spinning of Wearable Chitosan-Silica Textile for All-Day Radiative Cooling. *Chem. Eng. J.* **2023**, *475*, 146307. [CrossRef]
10. Yang, Z.; Zhang, J. Bioinspired Radiative Cooling Structure with Randomly Stacked Fibers for Efficient All-Day Passive Cooling. *ACS Appl. Mater. Interfaces* **2021**, *13*, 43387–43395. [CrossRef]
11. Song, Y.; Lei, M.; Lei, J.; Li, Z. A Scalable Hybrid Fiber and Its Textile with Pore and Wrinkle Structures for Passive Personal Cooling. *Adv. Mater. Technol.* **2020**, *5*, 2000287. [CrossRef]
12. Tian, Y.; Shao, H.; Liu, X.; Chen, F.; Li, Y.; Tang, C.; Zheng, Y. Superhydrophobic and Recyclable Cellulose-Fiber-Based Composites for High-Efficiency Passive Radiative Cooling. *ACS Appl. Mater. Interfaces* **2021**, *13*, 22521–22530. [CrossRef] [PubMed]
13. Li, T.; Zhai, Y.; He, S.; Gan, W.; Wei, Z.; Heidarinejad, M.; Dalgo, D.; Mi, R.; Zhao, X.; Song, J.; et al. A Radiative Cooling Structural Material. *Science* **2019**, *364*, 760–763. [CrossRef]
14. Zhong, S.; Yi, L.; Zhang, J.; Xu, T.; Xu, L.; Zhang, X.; Zuo, T.; Cai, Y. Self-Cleaning and Spectrally Selective Coating on Cotton Fabric for Passive Daytime Radiative Cooling. *Chem. Eng. J.* **2021**, *407*, 127104. [CrossRef]
15. Song, Y.-N.; Li, Y.; Yan, D.-X.; Lei, J.; Li, Z.-M. Novel Passive Cooling Composite Textile for Both Outdoor and Indoor Personal Thermal Management. *Compos. Part A Appl. Sci. Manuf.* **2020**, *130*, 105738. [CrossRef]
16. Wang, T.; Wu, X.; Zhu, Q.; Chen, Y.; Zhang, S.; Gu, M.; Zhang, Y. A Scalable and Durable Polydimethylsiloxane-Coated Nanoporous Polyethylene Textile for Daytime Radiative Cooling. *Nanophotonics* **2024**, *13*, 601–609. [CrossRef]
17. Zeng, S.; Pian, S.; Su, M.; Wang, Z.; Wu, M.; Liu, X.; Chen, M.; Xiang, Y.; Wu, J.; Zhang, M.; et al. Hierarchical-Morphology Metafabric for Scalable Passive Daytime Radiative Cooling. *Science* **2021**, *373*, 692–696. [CrossRef] [PubMed]
18. Ji, Y.; Sun, Y.; Muhammad, J.; Li, X.; Liu, Z.; Tu, P.; Wang, Y.; Cai, Z.; Xu, B. Fabrication of Hydrophobic Multilayered Fabric for Passive Daytime Radiative Cooling. *Macro. Mater. Eng.* **2022**, *307*, 2100795. [CrossRef]
19. Yang, R.; Yang, J.; Wang, M.; Xu, J.; Zhang, Y. Radiative Cooling Fabrics and Products. European Patent EP 3 819 425 A1, 2021.
20. Mandal, J.; Yang, Y.; Yu, N.; Raman, A.P. Paints as a Scalable and Effective Radiative Cooling Technology for Buildings. *Joule* **2020**, *4*, 1350–1356. [CrossRef]
21. Li, X.; Peoples, J.; Yao, P.; Ruan, X. Ultrawhite $BaSO_4$ Paints and Films for Remarkable Daytime Subambient Radiative Cooling. *ACS Appl. Mater. Interfaces* **2021**, *13*, 21733–21739. [CrossRef]
22. Gentle, A.R.; Smith, G.B. Radiative Heat Pumping from the Earth Using Surface Phonon Resonant Nanoparticles. *Nano Lett.* **2010**, *10*, 373–379. [CrossRef]
23. Kou, J.; Jurado, Z.; Chen, Z.; Fan, S.; Minnich, A.J. Daytime Radiative Cooling Using Near-Black Infrared Emitters. *ACS Photon.* **2017**, *4*, 626–630. [CrossRef]
24. Zhou, L.; Song, H.; Liang, J.; Singer, M.; Zhou, M.; Stegenburgs, E.; Zhang, N.; Xu, C.; Ng, T.; Yu, Z.; et al. A Polydimethylsiloxane-Coated Metal Structure for All-Day Radiative Cooling. *Nat. Sustain.* **2019**, *2*, 718–724. [CrossRef]
25. Woo, H.Y.; Choi, Y.; Chung, H.; Lee, D.W.; Paik, T. Colloidal Inorganic Nano- and Microparticles for Passive Daytime Radiative Cooling. *Nano Converg.* **2023**, *10*, 17. [CrossRef] [PubMed]
26. Smith, W.C. Metallized Fabrics—Techniques and Applications. *J. Coat. Fabr.* **1988**, *17*, 242–253. [CrossRef]
27. Manara, J.; Reidinger, M.; Rydzek, M.; Arduini-Schuster, M. Polymer-Based Pigmented Coatings on Flexible Substrates with Spectrally Selective Characteristics to Improve the Thermal Properties. *Prog. Org. Coat.* **2011**, *70*, 199–204. [CrossRef]
28. Bolm, H.; Rekowski, V.; Mardalen, J.; Hallestvet, M.; Jeffers, T. Low Emissive Powder Coating. US Patent US20070251420A1, 2007.
29. Luo, H.; Li, Q.; Du, K.; Xu, Z.; Zhu, H.; Liu, D.; Cai, L.; Ghosh, P.; Qiu, M. An Ultra-Thin Colored Textile with Simultaneous Solar and Passive Heating Abilities. *Nano Energy* **2019**, *65*, 103998. [CrossRef]
30. Houtman, R. Materials Used for Architectural Fabric Structures. In *Fabric Structures in Architecture*; Elsevier: Amsterdam, The Netherlands, 2015; pp. 101–121, ISBN 978-1-78242-233-4.
31. Cheng, H.; Wang, F.; Ou, J.; Li, W.; Xue, R. Solar Reflective Coatings with Luminescence and Self-Cleaning Function. *Surf. Interfaces* **2021**, *26*, 101325. [CrossRef]
32. Aili, A.; Wei, Z.Y.; Chen, Y.Z.; Zhao, D.L.; Yang, R.G.; Yin, X.B. Selection of Polymers with Functional Groups for Daytime Radiative Cooling. *Mater. Today Phys.* **2019**, *10*, 100127. [CrossRef]
33. Li, X.; Peoples, J.; Huang, Z.; Zhao, Z.; Qiu, J.; Ruan, X. Full Daytime Sub-Ambient Radiative Cooling in Commercial-like Paints with High Figure of Merit. *Cell Rep. Phys. Sci.* **2020**, *1*, 100221. [CrossRef]
34. Song, J.; Qin, J.; Qu, J.; Song, Z.; Zhang, W.; Xue, X.; Shi, Y.; Zhang, T.; Ji, W.; Zhang, R.; et al. The Effects of Particle Size Distribution on the Optical Properties of Titanium Dioxide Rutile Pigments and Their Applications in Cool Non-White Coatings. *Sol. Energy Mater. Sol. Cells* **2014**, *130*, 42–50. [CrossRef]
35. Mishra, B.R.; Sundaram, S.; Varghese, N.J.; Sasihithlu, K. Disordered Metamaterial Coating for Daytime Passive Radiative Cooling. *AIP Adv.* **2021**, *11*, 105218. [CrossRef]
36. *ASTM E903-20*; Standard Test Method for Solar Absorptance, Reflectance, and Transmittance of Materials Using Integrating Spheres. ASTM International: West Conshohocken, PA, USA, 2020. [CrossRef]
37. *ASTM C1044-16*; Practice for Using a Guarded-Hot-Plate Apparatus or Thin-Heater Apparatus in the Single-Sided Mode. ASTM International: West Conshohocken, PA, USA, 2016.
38. *Norm: DIN 52616:1977-11*; Wärmeschutztechnische Prüfungen; Bestimmung der Wärmeleitfähigkeit mit dem Wärmestrommeßplatten-Gerät. German Institute for Standardisation: Berlin, Germany, 2013.

39. Naghshine, B.B.; Saboonchi, A. Optimized Thin Film Coatings for Passive Radiative Cooling Applications. *Opt. Commun.* **2018**, *410*, 416–423. [CrossRef]
40. Wu, R.; Sui, C.; Chen, T.-H.; Zhou, Z.; Li, Q.; Yan, G.; Han, Y.; Liang, J.; Hung, P.-J.; Luo, E.; et al. Spectrally Engineered Textile for Radiative Cooling against Urban Heat Islands. *Science* **2024**, *384*, 1203–1212. [CrossRef] [PubMed]